Int. J. Appl. Ceram. Technol., 8 [6] 1382–1392 (2011)
DOI:10.1111/j.1744-7402.2010.02593.x

International Journal of
Applied Ceramic TECHNOLOGY
Ceramic Product Development and Commercialization

In-Flight Alloying of Nanocrystalline Yttria-Stabilized Zirconia Using Suspension Spray to Produce Ultra-Low Thermal Conductivity Thermal Barriers

Kent VanEvery,[§] Matthew John M. Krane, and Rodney W. Trice[*]

School of Materials Engineering, Purdue University, West Lafayette, Indiana 47907

Wallace Porter and Hsin Wang

Oak Ridge National Laboratory, Oak Ridge, Tennessee 37831-6064

Matthew Besser and Dan Sordelet[¶]

Ames Laboratory, Iowa State University, Ames, Iowa 50011-3020

Jan Ilavsky and Jonathan Almer

Argonne National Laboratory, Argonne, Illinois 60439

Major portions of this research were funded by the National Science Foundation via grant CMMI-0456534. This support is gratefully acknowledged. Ames Laboratory is operated for the U.S. Department of Energy by Iowa State University under Contract No. DE-AC02-07CH11358. Use of the Advanced Photon Source at Argonne National Laboratory was supported by the U.S. Department of Energy, Office of Science, Office of Basic Energy Sciences, under Contract No. DE-AC02-06CH11357. This project involved research sponsored by the Assistant Secretary for Energy Efficiency and Renewable Energy, Office of FreedomCAR and Vehicle Technologies, as part of the High Temperature Materials Laboratory User Program, Oak Ridge National Laboratory, managed by UT-Battelle, LLC, for the U.S. Department of Energy under contract number DE-AC05-00OR22725.
[*]rtrice@purdue.edu
[§]Present address: Progressive Surface, 4695 Danvers Dr. SE, Grand Rapids, Michigan 49512
[¶]Present address: Caterpillar Inc., Technical Center Bldg. E/854, 14009 Old Galena Road, Mossville, Illinois 61552

Previous researchers have shown that it is possible to combine rare-earth oxides with the standard thermal barrier coating material (4.5 mol% Y_2O_3–ZrO_2 or YSZ) to form ultra-low thermal conductivity coatings using a standard powder manufacturing route. A similar approach to making low thermal conductivity coatings by adding rare-earth oxides is discussed presently, but a different manufacturing route was used. This route involved dissolving hydrated ytterbium and neodymium nitrates into a suspension of 80 nm diameter 4.5 mol% YSZ powder and ethanol. Suspension plasma spray was then used to create coatings in which the YSZ powders were alloyed with rare-earth elements while the plasma transported the melted powders to the substrate. Mass spectrometry measurements showed a YSZ coating composition, in mol%, of ZrO_2–4.4 Y_2O_3–1.4 Nd_2O_3–1.3 Yb_2O_3. The amount of Yb^{3+} and Nd^{3+} ions in the final coating was ~50% of that added to the starting suspension. Wide-angle X-ray diffraction revealed a cubic ZrO_2 phase, consistent with the incorporation of more stabilizer into the zirconia crystal structure. The total porosity in the coatings was ~35–36%, with a bulk density of 3.94 g/cm^3. Small-angle X-ray scattering measured an apparent void specific surface area of ~2.68 m^2/cm^3 for the alloyed coating and ~3.19 m^2/cm^3 for the baseline coating. Thermal conductivity (k_{th}) of the alloyed coating was ~0.8 W/m/K at 800°C, as compared with ~1.5 W/m/K at 800°C for the YSZ-only baseline coating. After 50 h at 1200°C, k_{th} increased to ~1.1 W/m/K at 800°C for the alloyed samples, with an associated decrease in the apparent void specific surface area to ~1.55 m^2/cm^3.

Introduction

A means of increasing the efficiency of a gas turbine is to increase the temperature of the combustion gases entering the system.[1] In current commercial aircraft turbine engines, the gas temperature at the inlet is between 1000°C and 1300°C and eventually reaches a peak value that can exceed 1500°C.[2] However, the maximum operating temperature among the metallic components within a gas turbine is ~1100°C.[3] To reduce or prevent the degradation and failure of these parts, the metallic components must be protected from the heat flux produced by the combustion gases during engine operation. The protection typically used consists of two types—an internal airflow to cool the component convectively and a thermal barrier coating (TBC) deposited on the component to insulate it from the combustion heat flux. One of the key material properties for TBCs is thermal conductivity, which determines the capacity of the coating to insulate the underlying metallic structure. The industry standard TBC composition is 7–8 wt% Y_2O_3–ZrO_2 (YSZ), which is equivalent to ~4.5 mol%, because of the thermal conductivity (k_{th}) and thermal cycling performance of this ceramic.[4] Therefore, to increase further the efficiency of gas turbines, next-generation TBCs are needed that provide a lower k_{th} than 7–8 wt% YSZ while approximating the thermal cycling failure resistance of the current industry standard.

One method for lowering the thermal conductivity of YSZ-based thermal barriers is the defect clustering approach of Zhu and Miller.[5–8] Defect clustering involves doping baseline composition thermal barrier coatings with an equal molar ratio of paired rare-earth oxides such as Yb_2O_3 and Nd_2O_3. By incorporating paired rare-earth oxides into YSZ, Zhu and Miller have observed that thermodynamically stable, immobile oxide defect clusters are created. The clusters are designed to attenuate and scatter lattice phonon waves as well as scatter radiative photon waves. A 4.5 mol% YSZ coating containing defect clusters produced by Nd_2O_3 and Yb_2O_3 dopants at a combined stabilizer level of 9 mol% exhibited significant thermal conductivity differences from a baseline YSZ (no dopants added) coating.[6] Both the thermal conductivity and the rate at which the thermal conductivity increased in the ZrO_2–4.5 mol%Y_2O_3–4.5 mol% (Nd_2O_3+Yb_2O_3) coatings were significantly reduced compared with YSZ-only coatings. Other dopant pairs, such as Gd_2O_3–Yb_2O_3 and Gd_2O_3–Nd_2O_3, added to YSZ also demonstrated a lower thermal conductivity than coatings comprised of only YSZ.

In the Zhu and Miller work, individual batches of powders with the desired combination of YSZ and rare-earth oxides were spray-dried and then air plasma-sprayed to create coatings. In the work reported currently, similar coatings were generated via a new approach that combines a recently developed plasma spray process with defect clustering concepts. The spray process, called suspension plasma spray (SPS), involves first forming a colloidal suspension by dispersing nano-sized powders in a solvent containing a dissolved liquid dispersant. The dispersion of the powders in the suspension prevents agglomeration, a major obstacle when

spraying nanosized powders with a conventional air plasma spray (APS) process. The suspension is then sprayed into a plasma to evaporate the solvent and melt the powder. The plasma plume also propels the ceramic toward a substrate where the molten particles flatten upon impact, producing lamellae in a like manner to APS. However, because of the nanosize scale possible with SPS, a potential exists for ions adsorbed onto the surface of powder particles to alloy homogenously the molten droplets forming the coating. Therefore, this SPS alloying approach removes the need to synthesize individual batches of YSZ powders doped with each rare-earth oxide pair of interest. Instead, a single composition YSZ powder can be utilized to generate coatings with different compositions by altering the hydrated rare-earth nitrates dissolved in the suspension before spraying.

In this first study, two hydrated rare-earth nitrates, $Nd(NO_3)_3 \cdot 6H_2O$ and $Yb(NO_3)_3 \cdot 5H_2O$, were dissolved in suspensions containing 80 nm diameter 4.5 mol% YSZ powder. The goal was to produce a coating with a composition of ZrO_2–4.27 Y_2O_3–2.61 Nd_2O_3–2.61 Yb_2O_3, where the concentrations are in mol%. This composition was chosen because it exhibited the lowest thermal conductivity of those evaluated in the work of Zhu and Miller.[6] Subsequent coatings sprayed from the suspensions were shown to have Nd^{3+} and Yb^{3+} dopants within the zirconia lattice. Thermal conductivity measurements indicated a decrease in thermal conductivity for the alloyed YSZ coatings with respect to unalloyed YSZ-only coatings.

Experimental Procedure

Suspension Preparation

The suspensions utilized during this research contained ZrO_2 powder stabilized with 4.5 mol% ($\sim$8 wt%) Y_2O_3. The powder was synthesized by Inframat® Advanced Materials (Manchester, CT). In the as-received condition, the irregularly shaped, $\sim$80 nm diameter powder particles were agglomerated into 100 μm clusters. Ethanol was selected as the solvent for the suspensions based upon low toxicity, availability, and prior research.[9,10] Liquid phosphate ester (Triton® QS-44, Sigma-Aldrich, St. Louis, MO). was dissolved in the ethanol at a concentration of 1 wt% via mixing with a magnetic stir bar before the powder addition. Once the ethanol-dispersant solution was well-mixed, the YSZ powder was added at a concentration of either 2 or 8 wt%, and magnetic stir bar mixing was resumed to entrain the powder into the solvent. Baseline coatings were fabricated from suspensions containing only the YSZ powder.

The suspensions formulated to produce the ZrO_2–$(Y,Nd,Yb)_2O_3$ coatings included additions of $Nd(NO_3)_3 \cdot 6H_2O$ and $Yb(NO_3)_3 \cdot 5H_2O$ crystals, which were soluble in ethanol (Sigma-Aldrich® product numbers 289175 & 209147). The mass of each hydrated nitrate was added such that, if all of the Nd^{3+} and Yb^{3+} ions in the solvent were incorporated into the suspended YSZ, the resulting ceramic would have a composition of ZrO_2–4.27 Y_2O_3–2.61 Nd_2O_3–2.61 Yb_2O_3. Alloying agents were introduced following the powder entrainment in the solvent. Coatings evaluated in this study are designated as either 2P-AS-X, 2P-HT-X, 8PA-AS-X, or 8PA-HT-X. The first character indicates the suspension formulation in wt% of YSZ powder (either 2 or 8). The addition of a "PA" following the first character denotes a suspension of powder and rare earth nitrate alloying elements; whereas, "P" alone indicates a suspension of powder only. The "AS" or "HT" characters between the hyphens refer to whether the coating was evaluated in the as-sprayed or heat-treated conditions (50 h at 1200°C), respectively. The final character indicates the sample number.

Suspensions of only YSZ powders and those containing Nd/Yb nitrate additions along with the YSZ powders were milled to comminute the YSZ agglomerates and assist with homogenization. The grinding media utilized were 9.5 mm diameter by 9.5 mm long cylinders of dense YSZ. Optimum ball milling conditions were determined to be a jar rotation speed of 140 rpm for 3 h. The particle size distribution, as determined by a Beckman Coulter LS 230 particle analyzer (Fullerton, CA), showed a number-based d_{50} of 80 nm. Suspensions were made in 150 mL batches and often stored for >4 weeks before spraying.

Coating Production

During spraying, the suspension was contained in a 4 L 316 stainless steel pressure vessel placed on top of a magnetic stir plate, which rotated a 4-cm-long stir bar within the vessel to circulate the suspension and reduce particle settling. Additionally, to minimize the presence of settled agglomerates, all suspensions were manually

agitated, ultrasonicated for at least 15 min, and filtered through a 90 μm sieve before being added to the pressure vessel. A nitrogen back pressure of approximately 64 psig was used to force the suspension through a Teflon® fluorinated ethylene propylene supply line with a 1.6 mm internal diameter (Ozone Solutions, Hull, IA). The supply line terminated at a 230 μm diameter ruby injection nozzle (RB# 22016, Bird Precision, Waltham, MA). At 64 psig, the suspension was forced through the nozzle into the plume at a velocity of ~20.7 m/s. Prior work,[10] along with visual confirmation in the present study, revealed optimum entrainment of the suspension at this stream velocity. High-speed video revealed that the suspension entered the plasma as a stream.[11] Other researchers have shown that drag forces exerted by the plasma flow subsequently fragment the suspension stream into droplets.[12]

The plasma gun utilized during the SPS experiments was a Praxair® SG-100, located at Ames Laboratory (Praxair, Danbury, CT). The gun was operated in the subsonic mode at 50 kW (1000 A/50 V) with the 3083-129 cathode and the 3083-175 anode. The anode contained a port through which the suspension was injected orthogonal to the plasma as it flowed through the 6 mm diameter gun bore. The plasma flow followed a spiral motion due to the 3083-113 gas injector, which imparted a rotational component to the velocity of the plasma-forming gases entering the gap between the electrodes. For this study, the forming gases were argon and helium flowing at 20 and 60 slm, respectively.

The doped and undoped YSZ coatings were deposited onto flat electronic-grade copper substrates without a bond coat. The substrate plates were 0.5 mm thick × 2.5 cm wide × 10 cm long. The substrate surface to be coated was blasted with 24-grit alumina particles to increase the roughness and improve the adhesion of the YSZ coating. All substrates were ultrasonically cleaned in ethanol before coating application. The cleaned plate was then attached to the substrate holder, which was positioned such that the grit-blasted surface was 50 mm from the plasma gun face and orthogonal to the plasma flow exiting the gun. Airflow was focused behind the substrate to cool it during spraying. The velocity of air exiting each of the two 2.5 cm diameter cooling pipes was measured to be at least 30 m/s. Baffling was used to prevent the airflow from reaching the front of the substrate where the coating was being deposited. During all spray experiments, the plasma gun was attached to a simple translation robot that traveled horizontally at 29 cm/s. Each horizontal pass within a cycle was separated by a 3 mm vertical translation of the plasma gun downward. These vertical transitions occurred approximately 6 cm beyond the edges of the substrate front. Each coating cycle contained 14 horizontal passes, and experiments typically consisted of between 60 and 70 coating cycles. For an 8 wt% powder suspension, each cycle increased the coating thickness by ~6 μm.

Physical Characterization of Coatings

The bulk density of baseline and doped YSZ coatings was determined from a series of mass measurements based upon the methodology described in ASTM 373-88. A diamond impregnated core drill was used to make 12.7 mm diameter circular cuts through the coatings while they were still attached to the substrates. The copper substrates were then etched away with nitric acid, producing disk-shaped coating samples with a mass of ~0.2 g. Dry, saturated, and buoyant masses were recorded for each sample. All mass values during testing were determined to 0.0001 of a gram, and each type of mass measurement was repeated four times per sample, with the sample being removed from the balance so that it could be rezeroed between repetitions. From these measurements, bulk density and total porosity averages were calculated for each sample.

Thermal Conductivity Measurements

The circular samples used for density investigations were also used to measure the temperature-dependent thermal diffusivity exhibited by undoped and doped SPS coatings samples according to ASTM E 1461-01. These experiments occurred in the High Temperature Materials Laboratory (HTML) at Oak Ridge National Laboratory. The system at HTML used a fiber optic laser as the energy source. During testing, this laser was attached to a furnace with an Ar atmosphere that contained the coating samples and an infrared (IR) detector. Because zirconia is semitransparent to radiation with wavelengths near the IR portion of the electromagnetic spectrum,[13] the top and bottom surfaces of the coating samples were completely covered with colloidal graphite before testing. This graphite covering absorbed the incident laser radiation so that the heat transfer through the coating occurred only by conduction. Conduction occurs by lattice vibrations, which produce phonons that travel at

the speed of sound in the material; whereas, radiation occurs by the motion of photons that travel at the speed of light.[14,15] Consequently, without the graphite layer, the transparency of the YSZ to the incident radiation would cause an increase in the energy detected by the IR sensor that would be falsely high relative to the specimen conduction resistance. The conduction resistance through the graphite covering is assumed to be negligible relative to that through the coating sample because the thermal conductivity of graphite is approximately ten times that of dense YSZ.[16]

Two furnace–detector setups were used to evaluate the coating thermal diffusivity over a temperature range consistent with gas turbine operation. The first furnace featured an InSb detector and was used for measurements from 200°C to 500°C. The second furnace featured an Si detector and was used for measurements from 700°C to 1200°C. The measurements were recorded at 100°C intervals over both temperature ranges. A computer controlled the testing procedure and automatically calculated average thermal diffusivity values from the sample thickness input by the user and three consecutive IR detector data sets collected at the measurement temperature. These calculations included corrections for radiation losses determined from the work of Clark and Taylor.[17] Thermal diffusivity for undoped and doped samples was measured in the as-sprayed condition and after a 50-h heat treatment at 1200°C in air.

Each average thermal diffusivity were converted to a thermal conductivity by multiplying these measurements with the average bulk density of each test specimen and the constant pressure heat capacity (c_p) of 4.5 mol% Y_2O_3–ZrO_2 at the measurement temperature. The temperature-dependent c_p data for 4.5 mol% YSZ were determined from differential scanning calorimetry experiments performed by researchers at HTML.[18] The neodymia and ytterbia additions in the alloyed YSZ coatings were assumed not to affect the constant pressure heat capacity of the ceramic; however, their effect will be investigated in future studies.

X-Ray Investigations

The structures of the coatings were characterized in a series of experiments involving a beam of ~80 keV X-rays from the synchrotron radiation source in the Advanced Photon Source facility at Argonne National Laboratory (ANL). This characterization involved using the portions of the beam that were absorbed by and transmitted through coating sections to study the atomic structure and microstructure of baseline and doped YSZ coatings. Each 1-mm-wide coating section was obtained by making parallel cuts along the diameter of a thermal diffusivity test specimen. The graphite coverings were removed from these test specimens by heating them in air at 500°C for 5 h before cutting. For the X-ray measurements, each coating section was oriented such that the beam direction was perpendicular to the coating spray direction and normal to the cross-sectional surfaces produced by cutting the thermal diffusivity test specimen. The volume of each coating section investigated with X-rays was the coating thickness (nominally 380 ± 40 μm) × 500 μm × 1000 μm. To sample this representative volume, the 30 μm high, 100 μm wide beam was sequentially positioned across the height of the coating section along a vertical line of locations. A total of five such vertical scans were conducted on each coating section with a 100 μm horizontal distance separating the centerlines of adjacent scans. This scanning process was performed three times on each coating section to collect absorption, wide-angle scattering, and small-angle scattering data.

X-Ray Absorption Experiments: The volume percent of total porosity, which included both open and closed types, in the coating sections was determined from the X-ray intensity data collected during the absorption scans. The intensity of the beam was recorded both before and after the sample at each position in the scan. For each sample, the intensity values corresponding to when the beam was positioned entirely on the coating section were averaged and divided by the intensity at a position for which the beam had no interaction with the ceramic. The negative natural logarithm of the result was then divided by the average coating section width over the scanned volume to give an absorption coefficient.[19] The porosity within the coating is expected to decrease the value of this coefficient below the value corresponding to the theoretical absorbance of the ceramic.[19] Using compositional data from WAXS experiments (described below) and elemental absorption coefficients from the NIST database,[20] the theoretical absorption coefficient for each test specimen was computed. The volume percent of total porosity, χ, was then calculated using:

$$\chi = 1 - \frac{\varepsilon_{ex}}{\varepsilon_{theo}} \quad (1)$$

where ε_{ex} represents the experiment absorption coefficient and ε_{theo} represents the theoretical absorption

coefficient. Values of 0.67 and 0.81 were determined for the ε_{theo} coefficients of the undoped YSZ and doped YSZ coatings, respectively (J. Almer, Argonne National Laboratory, personal communication).

Wide-Angle X-Ray Scattering (WAXS) Experiments: WAXS measurements were used to determine the atomic crystal structure of each coating section. These measurements consisted of recording the scattering of transmitted X-rays on an area detector located ~1.3 m behind the sample. The crystalline phases relevant to current YSZ TBCs are the nonequilibrium composition tetragonal (identified here as t'-ZrO_2), equilibrium composition tetragonal (t-ZrO_2), and cubic (c-ZrO_2) zirconia. All three crystal structures are identified by diffraction from the (004) and (400) planes. On an intensity vs 2θ diffraction plot, the peaks corresponding to the (004) and (400) planes of the tetragonal phases will appear at lower and higher angles, respectively, than the peak from the {400} planes of the cubic phase. For 4.5 mol% Y_2O_3–ZrO_2 plasma-sprayed coatings, the unit cell parameters have been reported to be $a = b = 5.11$ Å and $c = 5.16$ Å for the t'-ZrO_2 structure and $a = b = c = 5.136$ Å for c-ZrO_2.[21–23] The lattice parameters for the equilibrium tetragonal phase are $a = b = 5.096$ Å and $c = 5.18$ Å.[22]

By comparing the WAXS results from a ceria powder standard to a theoretically calculated diffraction pattern for this material, the FIT2D program[24] established the detector alignment relative to the scattered radiation (Debye cones). The resulting correction factors were adjusted to improve the alignment of the diffraction peaks from 4.5 mol% Y_2O_3–ZrO_2 samples to the corresponding 2θ locations published in Muraleedharan *et al.*[22] The diffraction data were averaged over the full 360° measured, to produce one-dimensional intensity vs 2θ plots for each sample. This averaging increased signal sensitivity allowing the appearance of shoulders on the peaks to be more readily detected than for conventional point-detector data.

Small-Angle X-Ray Scattering (SAXS) Experiments: In the case of plasma-sprayed microstructures, like those in SPS coatings, the electron density difference at the interfaces between the ceramic and the gas within voids generates coherently scattered X-rays at small angles.[25,26] Thus, SAXS was used in the current study to investigate microstructural differences between undoped and doped SPS coatings. For these experiments, a two-dimensional charge-coupled detector (CCD) located approximately 5 m behind the sample was used to measure the intensity as a function of a scattering wave vector, $\vec{q}$. At large $\vec{q}$ values, the SAXS data exhibit an annular region where the scattered intensity is inversely proportional to the magnitude of $\vec{q}$ raised to the fourth power. This relationship between intensity and $\vec{q}$ is commonly referred to as the Porod scattering regime.[19,26–28] The intensities within the Porod regime mainly result from X-rays experiencing a single scattering event as they passed through the sample.[28] Because an X-ray contributing to the Porod regime intensities typically does not interact with multiple cracks or pores, a Porod constant can be calculated from these intensities and related to the void specific surface area within the sample.[26,27] When determining the apparent total void specific surface area of a sample, an average Porod constant was calculated over one quarter of the annular intensity region exhibiting Porod scattering regime behavior. The qualifier apparent is applied to this area because SAXS experiments were not performed with multiple sample orientations to verify the actual total void specific surface area in a coating.[27] However, prior work has demonstrated that plasma-sprayed microstructures exhibit rotational symmetry about a spray direction that is orthogonal to the substrate during deposition.[26] Based upon this finding, SAXS from a single sample orientation in which the beam is perpendicular to this spray direction can provide an accurate representation of the void specific surface area in a plasma-sprayed coating. The same quarter annulus of intensity data was subdivided into a series of 5° segments, and an average Porod constant was determined for each segment. When plotted on a polar graph, these segment Porod constants show how the void specific surface area varies with orientation in a plane perpendicular to the direction of the X-ray beam passed through the sample.

Results and Discussion

Coating Overview and Crystal Structure

As presented in Table I, doped coatings in the as-sprayed condition demonstrated total porosities of approximately 35–36 vol%. After heat treating for 50 h at 1200°C, the total porosity values mostly remained within the uncertainty limits of the measurements. Table I also shows that the porosities determined by the immersion method compared well with those

Table I. Bulk Density and Porosity Data Corresponding to the Thermal Conductivity Results Plotted in Fig. 2

		Total porosity (vol%)	
Coating Sample	**Bulk density (g/cm^3)**	**Immersion method**	**X-ray absorption method**
8PA-AS-1	3.88 ± 0.06	36 ± 1	40 ± 1
8PA-AS-2	3.98 ± 0.06	35 ± 2	35 ± 2
8PA-HT-1	4.14 ± 0.12	35 ± 4	34 ± 2
8PA-HT-2	4.11 ± 0.10	34 ± 3	31 ± 1
2P-AS-1	3.92 ± 0.06	37 ± 2	—
2P-AS-2	4.20 ± 0.08	31 ± 2	—

AS, as-sprayed; HT, heat treated.

determined by X-ray absorption. Undoped coatings made from suspensions containing only 2 wt% YSZ powders in ethanol were compared with the doped coatings produced from 8 wt% powder suspensions because of the similarities in bulk densities. Figure 1 shows SEM micrographs of a YSZ-only coating (2P) and a YSZ plus dopant coating (8PA) in cross section. Comparison of the images reveals similar microstructures for each coating type.

Inductively coupled plasma techniques (NSL Analytical, Cleveland, OH) were used to quantify the mass fractions of Nd, Y, Yb, and Zr incorporated into the doped coating. This analysis determined the ceramic composition in mol% to be ZrO_2–4.4 Y_2O_3–1.4 Nd_2O_3–1.3 Yb_2O_3. According to this result, half of the neodymium and ytterbium added to the suspension was incorporated in the coating. An elemental composition map (not shown) obtained from energy-dispersive spectroscopy on a doped coating indicated an even distribution of Nd and Yb atoms.

Diffraction spectra representative of the WAXS data for the doped coating samples are displayed in Fig. 2. The WAXS data from an undoped sample are also plotted in this figure to provide a reference for the diffraction spectrum of a ZrO_2–4.5 mol% Y_2O_3 coating. As with the results of Zhu *et al.*,[8] the YSZ coating containing Nd and Yb atoms did not display the split (004) and (400) peaks associated with either of the tetragonal zirconia phases typically observed in plasma-sprayed YSZ coatings.[22] Instead, a central peak corresponding to the {400} cubic zirconia planes is present for the doped coating. This result would be expected for the case where Nd^{3+} and Yb^{3+} ions substitute into the zirconia lattice, stabilizing the cubic structure.[8]

An estimate of the Yb^{3+} or Nd^{3+} diffusion distance into YSZ is given by $\sqrt{Dt}$ where D is the diffusion coefficient in cm^2/s and t is the time in seconds. If the velocity of the powder in the plume is 200 m/s,[29] and the spray distance is 5 cm, then the resident time of the powder in the plume is ~0.25 ms. In a study by Kilo *et al.*,[30] they measured a diffusion coefficient of $\sim 10^{-12}$ cm^2/s at 1650°C for Y^{3+} diffusing into *crystalline* 10 mol% Y_2O_3–ZrO_2 using radio-active tracers. In terms of ionic radius, Y (ionic radius of 0.090 nm) is similar in size to Nd^{3+} (0.098 nm) and Yb^{3+} (0.087 nm).[31] Use of this diffusion coefficient with the 0.13 ms powder resident time gives an estimated diffusion depth of 0.16 nm, much less than the starting 80 nm diameter YSZ powders. However, the value for D used is too low because the actual diffusion coefficient in *melted* zirconia would be orders of magnitude higher. From Fig. 1, the feature size capable of being alloyed appears to be 500 nm to 1 μm. However, extensive TEM analysis would be required to determine the location of the dopants and whether they are predominantly located around the exterior of the microstructural features (i.e., due to limited diffusion into the melted powder) or homogenously distributed. These detailed microscopy experiments are planned.

Closer examination of Fig. 2 reveals a shoulder near 6.45° in the doped spectrum, suggesting that these data may result from the partial overlap of two peaks—one centered at ~6.43° and one centered at ~6.45°. Two peaks could be caused by the existence of preferred cation combinations among the possible compositions of an alloyed unit cell. Cation segregation has been reported for ZrO_2–$(Nd,Y,Yb)_2O_3$ ceramics.[6,8] This

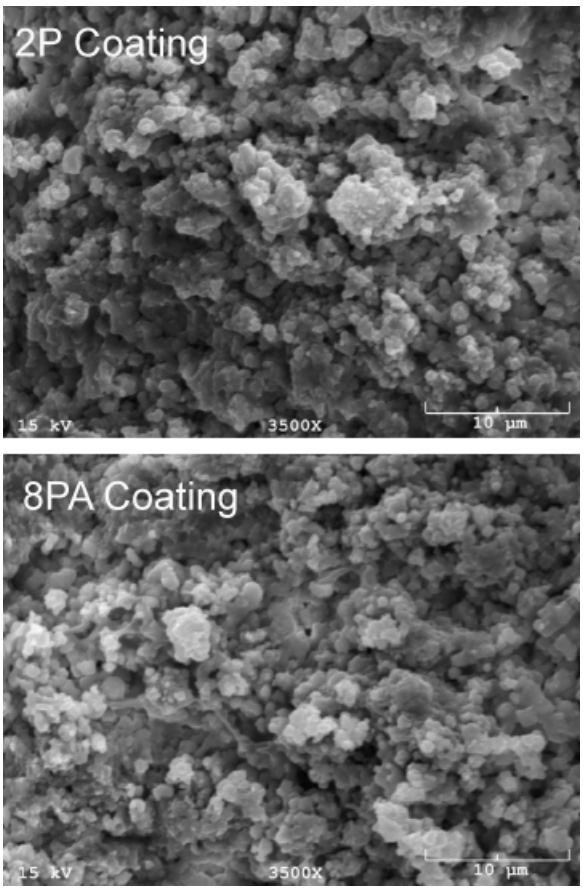

Fig. 1. Cross-sectional SEM images comparing SPS coatings made from undoped and doped coatings. The starting powder for both coatings was 50 nm YSZ. Doped coatings contained Nd and Yb atoms.

segregation is believed to be caused by the size differences between the Nd^{3+}, Y^{+3}, and Yb^{3+} species.[6,8]

After a 50-h heat treatment at 1200°C, only minor changes in the WAXS data were observed in the alloyed coating. No peaks corresponding to the formation of a monoclinic ZrO_2 phase were found on the WAXS spectrum after heat treatment, indicating that the phase assemblage of the coating is at least stable for this heat treatment.

Thermal Conductivity of Alloyed Coatings

Figure 3 shows the as-sprayed and heat-treated thermal conductivity (k_{th}) versus temperature data for the SPS coatings fabricated from nanopowder YSZ suspensions containing neodymium and ytterbium nitrates

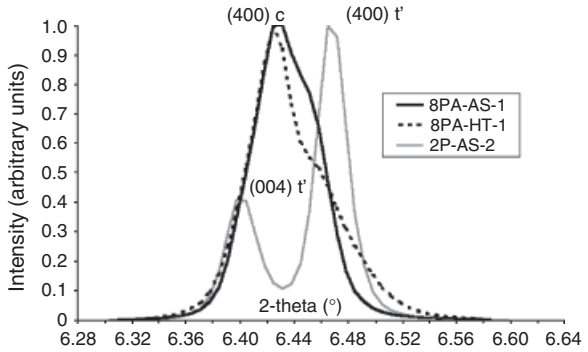

Fig. 2. Intensity (arbitrary units) vs 2Θ spectra showing the diffraction of 0.1442 Å wavelength X-rays from the (400) planes of the cubic (c) zirconia phase in doped coating samples (8PA-AS-1 and 8PA-HT-1), and from the (004) and (400) planes of the nonequilibrium tetragonal (t′) zirconia phase in an undoped sample (2P-AS-2).

dissolved in the solvent. Data for the unalloyed 2P coating are also plotted on Fig. 3 because, as shown in Table I, this coating exhibited similar total porosities as the alloyed 8PA coating in both the as-sprayed (AS) and heat-treated (HT) conditions. For all temperatures

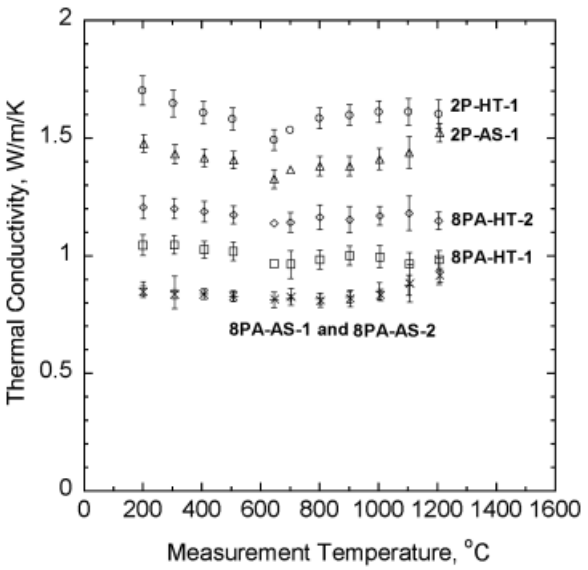

Fig. 3. Thermal conductivity versus temperature data for as-sprayed (8PA-AS) and heat-treated (8PA-HT) coating samples produced using an 8 wt% nanopowder suspension containing dissolved Nd and Yb nitrates, along with corresponding data (2P-AS, 2P-HT) for coating samples produced using a 2 wt% nanopowder suspension that did not contain dissolved Nd and Yb nitrates.

investigated, the alloyed samples demonstrated lower thermal conductivities than the nonalloyed samples, independent of coating condition (i.e., as-sprayed or heat treated). At 800°C for example, the as-sprayed alloyed samples demonstrated a k_{th} of 0.8 W/m/K, as compared with a k_{th} of 1.4 W/m/K for the as-sprayed unalloyed coating.

From 200°C to 500°C, the 8PA samples exhibited a smaller thermal conductivity decrease than the 2P samples. This finding indicates that lattice vibrations constituted a smaller percentage of the overall resistance to phonon transport within the alloyed samples, which is consistent with the lattice changes associated with the Nd^{3+} and Yb^{3+} additions increasing the total phonon scattering in the coating. From 900°C to 1200°C, the alloyed and unalloyed AS thermal conductivity data in Fig. 2 show similar temperature dependence. Cracks and pores in YSZ have been observed to sinter above 1000°C.[27] Therefore, alloying did not significantly affect the sintering behavior of the SPS microstructure. The reduction or absence of a thermal conductivity increase in the heat-treated data for either coating type between 900°C and 1200°C is the result of the heat treatment reducing the driving force for sintering within the coatings.

The difference in average thermal conductivity between the alloyed and nonalloyed coatings can be due to a variety of factors, including the phase assemblage in the coating, the shape and amount of porosity, and residual lattice strains. Each of these mechanisms contributes to increased phonon scattering in the coating. In terms of phase assemblage, the presence of a c-ZrO_2 peak in the alloyed WAXS results in place of the t'-ZrO_2 peaks observed for the yttria-only-stabilized zirconia coatings demonstrates that, at a minimum, Nd^{3+} and Yb^{3+} dopants have been incorporated into the YSZ structure. The cubic structure would be expected to have a lower k_{th} because of the increased amount of vacancies associated with the additional aliovalent cation(s) required to stabilize this phase in zirconia. For example, Raghavan *et al.*[32] showed that 98% dense c-ZrO_2 has a k_{th} of 2.3 W/m/K at 800°C; whereas, 98% dense tetragonal zirconia exhibits a thermal conductivity of 2.6 W/m/K at the same temperature. Thus, the presence of c-ZrO_2 appears to contribute to lowering alloyed coating thermal conductivity below that of the nonalloyed coating. But the phase assemblage change alone does not fully explain the ~0.6 W/m/K difference in the average thermal conductivity observed between the unalloyed 2P-AS-1 and the alloyed 8PA-AS coatings.

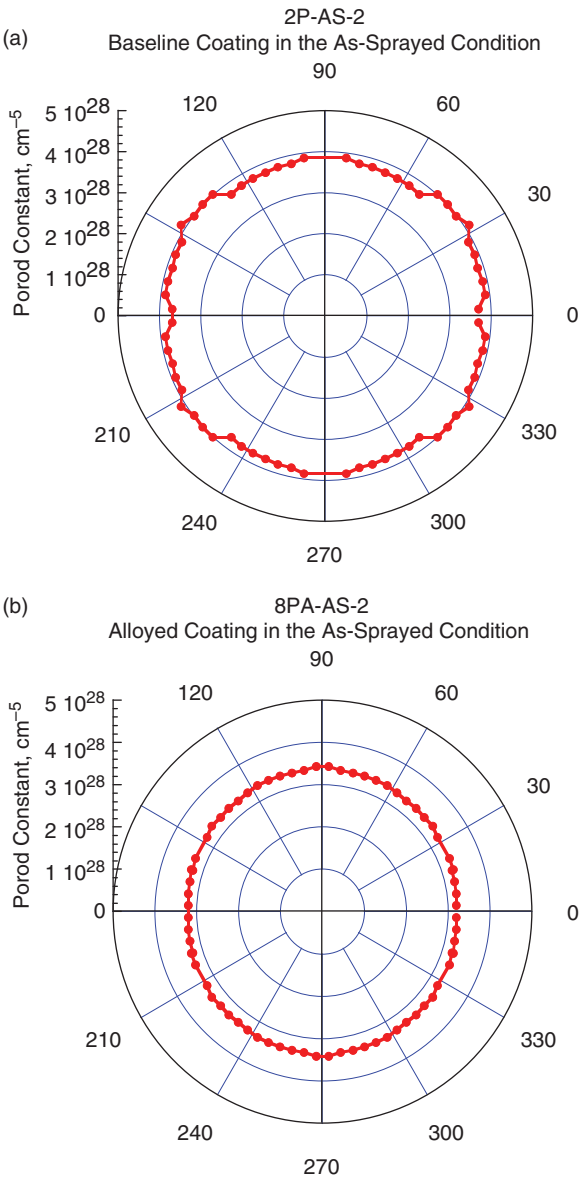

Fig. 4. Polar plots of Porod constant versus azimuthal angle for the (a) 2P-AS-2 and (b) 8PA-AS-2 samples.

The porosity orientation can also play a role in reducing the thermal conductivity of a coating. For example, a lenticular-shaped pore oriented perpendicular to the heat flow provides more resistance to phonon transport than if the pore is aligned with the heat flow. The porosity orientation in the doped and undoped

coatings was estimated using the azimuthal dependence of the Porod constants determined from the SAXS investigations. Polar plots showing this dependence in the 2P-AS-2 and 8PA-AS-2 samples can be seen in Fig. 4. Both plots in Fig. 4 show a roughly circular shape, meaning that the combined surface area from the cracks and pores in each coating did not exhibit anisotropy. The SAXS results also revealed that the 2P-AS coating contained a larger apparent void specific surface area (Table II). Because these coatings contained approximately the same amount of total porosity (Table I), the data in Table II indicate that the voids in the 2P-AS coating were distributed in a manner that increased the void/solid interfacial area. For example, the average pore size in the 2P-AS coating may have had a smaller diameter than that in the 8PA-AS coating. Given the orientation similarity in these two coatings, an increase in the pore/solid interfacial area would increase phonon scattering, yet the thermal conductivity of the 2P-AS sample was higher than that of the 8PA-AS samples. Thus, it can be concluded from the SAXS and density data that the difference in thermal conductivity between the unalloyed and alloyed samples is not the result of differences in the amount, size, or orientation of the porosity within the coatings.

Lattice strains scatter phonons traveling through a ceramic, thus lowering the k_{th} of a coating.[6,8,14] Clearly, the differences in radii of zirconia-stabilizing elements introduced in the alloyed coatings of the current study will increase the lattice strain in these ceramics above that present in the baseline YSZ coatings. Additionally, the WAXS results presented above suggest that the atomic structure of an alloyed coating could contain various sizes and types of unit cells—a condition that would produce further strain in the zirconia lattice. (A thorough TEM investigation is required to verify this condition, and such an investigation will be conducted as part of ongoing research into alloyed SPS YSZ coatings that has recently received funding.) However, as mentioned above, strain in the form of oxygen vacancies was also introduced during alloying due to the incorporation of additional aliovalent cations into the zirconia lattice. Therefore, to understand the effects of the neodymium and ytterbium dopants on coating thermal conductivity, the k_{th} differences between the 2P-AS and the 8PA-AS samples must be separated into contributions associated with increasing the oxygen vacancy concentration and contributions resulting from the rare-earth ion defects. Zhu and Miller.[6] examined the thermal conductivity of three zirconia-based ceramics: ZrO_2–4.5 Y_2O_3, ZrO_2–10 Y_2O_3, and ZrO_2–4.5 Y_2O_3–2.75 Nd_2O_3–2.75 Yb_2O_3, where the concentrations are in mol%, and found the respective thermal conductivities to be 1.4, 0.88, and 0.5 W/m/K.[5] The radii of yttrium and zirconium ions vary by approximately 3%.[33] As a result, the thermal conductivity difference between a ZrO_2–4.5 Y_2O_3 and a ZrO_2–10 Y_2O_3 ceramic is more likely due to the lattice strain increase accompanying the introduction of more oxygen vacancies than the strain produced by the substitution of Y^{3+} ions on Zr^{2+} lattice sites. Hence, in the prior work of Zhu and Miller,[6] the increase in oxygen vacancies generated by increasing the yttria stabilizer content from 4.5 to 10 mol% reduced k_{th} by 0.52 W/m/K. When the trivalent stabilizer content in the same study was increased from 4.5 to 10 mol% through Nd and Yb additions, the k_{th} deceased by 0.9 W/m/K. Consequently, based upon the preceding porosity discussion and the findings of Zhu and Miller,[6] an estimated 60% of the thermal conductivity decrease between the 2P-AS and 8PA-AS samples can be attributed to the oxygen vacancy concentration increase accompanying alloying, with the lattice distortions produced by the Nd^{3+} and Yb^{3+} ion substitutions comprising the remaining 40%.

A comparison of the data in Fig. 3 from heat-treated specimens shows that, although the thermal conductivity of the 8PA-HT samples did increase relative to the 8PA-AS samples, the alloyed YSZ still exhibited a lower thermal conductivity than the unalloyed YSZ after 50 h at 1200°C. The WAXS data in Fig. 2, the bulk density data in Table I, and the apparent void specific surface areas in Table II for the alloyed samples indicate

Table II. Total Apparent Void Specific Surface Areas for an As-Sprayed Baseline (Undoped) SPS YSZ Sample and Samples Alloyed with Nd^{3+} and Yb^{3+} in the As-Sprayed and Heat-Treated (50 h at 1200°C) Conditions

Coating sample	Apparent total void specific surface area (m^2/cm^3)
8PA-AS-1	2.72 ± 0.17
8PA-AS-2	2.65 ± 0.11
8PA-HT-1	1.67 ± 0.05
8PA-HT-2	1.43 ± 0.09
2P-AS-2	3.19 ± 0.07

AS, as-sprayed; HT, heat treated; SPS, suspension plasma spray.

that the thermal conductivity increase following the heat treatment was more probably the result of sintering affecting the coating porosity than atomic diffusion changing the crystal structure. This conclusion is supported by the similar thermal conductivity increase between the 2P-AS and 2P-HT data plotted on Fig. 3.

Summary and Conclusions

A suspension containing YSZ powder and dissolved neodymium and ytterbium nitrates generated a ZrO_2–4.4 Y_2O_3–1.4 Nd_2O_3–1.3 Yb_2O_3 (concentrations in mol%) coating that was tested in the as-sprayed and heat-treated states. The addition of the Nd and Yb alloying elements raised the oxygen vacancy concentration and is believed to have introduced substitution atom strains into the zirconia lattice. These effects combined to reduce the coating thermal conductivity. In both the as-sprayed and heat-treated conditions, the thermal conductivity of the coating alloyed with Nd and Yb was $\sim$0.6 W/m/K lower than that of a YSZ SPS specimen having approximately the same porosity characteristics. These findings agree with previous research[6] on APS coatings produced from ZrO_2–4.5 Y_2O_3–2.75 Nd_2O_3–2.75 Yb_2O_3 (concentrations in mol%) powder. The results indicate that SPS can be used to tailor the final coating composition by simply adjusting the composition of the starting suspension.

References

1. A. Portinha, *et al.*, "Characterization of Thermal Barrier Coatings with a Gradient in Porosity," *Surf. Coat. Technol.*, 195 245–251 (2005).
2. W. Beele, G. Marijnissen, and A. Van Lieshout, "The Evolution of Thermal Barrier Coatings—Status and Upcoming Solutions for Today's Key Issues," *Surf. Coat.Technol.*, 120–121 61–67 (1999).
3. U. Schulz, *et al.*, "Some Recent Trends in Research and Technology of Advanced Thermal Barrier Coatings," *Aerospace Sci. Technol.*, 7 73–80 (2003).
4. R. A. Miller, "Thermal Barrier Coatings for Aircraft Engines: History and Directions," *J. Therm. Spray Tech.*, 6 [1] 35–42 (1997).
5. D. Zhu and R. A. Miller, "Low Conductivity and Sintering-Resistant Thermal Barrier Coatings," U.S. Patent #20,050,026,770, 2005.
6. D. Zhu and R. A. Miller, "Development of Advanced Low Conductivity Thermal Barrier Coatings," *Int. J. Appl.Ceram. Technol.*, 1 [1] 86–94 (2004).
7. D. Zhu and R. A. Miller, "Thermal Conductivity and Sintering Behavior of Advanced Thermal Barrier Coatings," *Ceram. Eng. Sci. Proc.*, 23 457–468 (2002).
8. D. Zhu, Y. L. Chen, and R. A. Miller, "Defect Clustering and Nano-Phase Structure Characterization of Multicomponent Rare-Earth Oxide Doped Zirconia-Yttria Thermal Barrier Coatings," *Ceram. Eng. Sci. Proc.*, 24 525–534 (2003).
9. Z. Chen, R. W. Trice, M. Besser, X. Yang, and D. Sordelet, "Air Plasma Spraying Colloidal Solutions of Nanosized Ceramic Powders," *J. Mater. Sci.*, 39 4171–4178 (2004).
10. R. Siegert, "A Novel Process for the Liquid Feedstock Plasma Spray of Ceramic Coatings with Nanostructural Features," Doctoral Thesis, Institut fur Werkstoffe und Verfahren der Energietechnik, 2005.
11. K. Van Every, "Development and Evaluation of Suspension Plasma Sprayed Yttria Stabilized Zirconia Coatings for Thermal Barriers," Ph.D. Thesis, School of Materials Engineering, Purdue University, May 2009.
12. J. Fazilleau, C. Delbos, V. Rat, J. F. Coudert, P. Fauchais, and B. Pateyron, "Phenomena Involved in Suspension Plasma-Spraying, Part 1: Suspension Injection and Behavior," *Plasma Chem. Plasma Process*, 26 371–391 (2006).
13. B. Nait-Ali, K. Haberko, H. Vesteghema, J. Absi, and D. S. Smith, "Thermal Conductivity of Highly Porous Zirconia," *J.Eur. Ceram. Soc.*, 26 3567–3574 (2006).
14. J. R. Nicholls, K. J. Lawson, A. Johnstone, and D. S. Rickerby, "Methods to Reduce the Thermal Conductivity of EB-PVD TBCs," *Surf. Coat. Technol.*, 151–152 383–391 (2002).
15. P. K. Schelling and S. R. Phillpot, "Mechanism of Thermal Transport in Zirconia and Yttria-Stabilized Zirconia by Molecular-Dynamics Simulation," *J. Am. Ceram. Soc.*, 84 [12] 2997–3007 (2001).
16. D. S. Almeida, C. R. M. Silva, M. C. A. Nonob, and C. A. A. Cairo, "Thermal Conductivity Investigation of Zirconia Co-Doped with Yttria and Niobia EB-PVD TBCs," *Mater. Sci. Eng. A*, 443 60–65 (2007).
17. L. M. Clark III and R. E. Taylor, "Radiation Loss in the Flash Method for Thermal Diffusivity," *J. Appl. Phys.*, 46 [2] 714–719 (1975).
18. W. D. Porter, *Differential Scanning Calorimetry Data for ZrO_2–8 wt% Y_2O_3.* Oak Ridge National Laboratory, Oak Ridge, TN, 2006.
19. A. A. Kulkarni, *et al.*, "Depth Resolved Porosity Investigation of EB-PVD Thermal Barrier Coatings Using High Energy X-Rays," *J. Am. Ceram. Soc.*, 87 [2] 268–274 (2004).
20. E. B. Saloman, J. H. Hubbell, and J. H. Scofield, "X-Ray Attenuation Cross Sections for Energies 100 eV to 100 keV and Elements Z = 1 to = 92. Atomic Data and Nuclear Data Tables," At. Data Nucl. Data Tables, 38 1–197 (1988).
21. G. Witz, V. Shklover, W. Steurer, S. Bachegowda, and H. -P. Bossmann, "Phase Evolution in Yttria-Stabilized Zirconia Thermal Barrier Coatings Studied by Rietveld Refinement of X-Ray Powder Diffraction Patterns," *J. Am. Ceram. Soc.*, 90 [9] 2935–2940 (2007).
22. K. Muraleedharan, J. Subrahmanyam, and S. B. Bhaduri, "Identification of t′ Phase in ZrO_2–7.5 wt% Y_20_3 Thermal-Barrier Coatings," *J. Am. Ceram. Soc.*, 71 [5] C226–C227 (1998).
23. J. Ilavsky and J.K Stalick, "Phase Composition and its Changes During Annealing of Plasma Sprayed YSZ," *Surf. Coat. Technol.*, 127 120–129 (2000).
24. A. P. Hammersley, "FIT2D V9.129 Reference Manual V3.1," *ESRF Internal Report ESRF98HA01T*, 1998.
25. A. Kulkarni, *et al.*, "Comprehensive Microstructural Characterization and Predictive Property Modeling of Plasma-Sprayed Zirconia Coatings," *Acta Mater.*, 51 2457–2475 (2003).
26. J. Ilavsky, A. J. Allen, G. G. Long, S. Krueger, C. C. Berndt, and H. Herman, "Influence of Spray Angle on the Pore and Crack Microstructure of Plasma-Sprayed Deposits," *J. Am. Ceram. Soc.*, 80 [3] 733–742 (1997).
27. J. Ilavsky, G. G. Long, A. J. Allen, and C. C. Berndt, "Evolution of the Void Structure in Plasma-Sprayed YSZ Deposits During Heating," *Mater. Sci. Eng. A*, 272 215–221 (1999).
28. O. Glatter and O. Kratky, *Small Angle X-Ray Scattering*, Academic Press, New York, 1982.
29. J. F. Bisson, B. Gautheir, and C. Moreau, "Effect of Plasma Fluctuations on In-Flight Particle Parameters," *J. Therm. Spray Tech.*, 12 [1] 38–43 (2003).
30. M. Kilo, *et al.*, "Cation Self-Diffusion of 44Ca, 88Y, and 96Zr in Single-Crystalline Calcia- and Yttria-Doped Zirconia," *J. Appl. Phys.*, 94 [12] 7547–7552 (2003).
31. Y. -M. Chiang, D. Birnie III, and W. D. Kingery, *Physical Ceramics: Principles for Ceramic Science and Engineering*, Wiley Press, New York, 1997, p. 15.
32. S. Raghavan, H. Wang, R. B. Dinwiddie, W. D. Porter, and M. Mayo, "The Effect of Grain Size, Porosity, and Yttria Content on the Thermal Conductivity of Nanocrystalline Zirconia," *Scr. Mater.*, 38 [8] 1119–1125 (1998).
33. Flinn Scientific Inc. *Flinn Scientific Periodic Table of Elements*, Flinn Scientific, Batavia, IL, 1996.